



Time-dependent inversion of three-component continuous GPS for steady and transient sources in northern Cascadia

Robert McCaffrey¹

Received 1 December 2008; revised 29 January 2009; accepted 6 February 2009; published 3 April 2009.

[1] An approach to invert GPS time series to estimate crustal block rotations, fault locking and strain rates while simultaneously solving for transient slow slip events is described and applied to the northern Cascadia subduction zone. The method can use continuous or survey mode GPS time series or both. I invert 5.6 years of 3-component continuous GPS time series at 53 sites from Cascadia to estimate simultaneously the block motions and strains, locking on the subduction zone and source parameters of the four most recent slow-slip events. Over the time period and section of the Cascadia margin sampled, the strain released in slow slip was 7 to 10% of the accumulated subduction strain but at the base of and immediately down dip of the locked zone beneath the Olympic Peninsula. **Citation:** McCaffrey, R. (2009), Time-dependent inversion of three-component continuous GPS for steady and transient sources in northern Cascadia, *Geophys. Res. Lett.*, 36, L07304, doi:10.1029/2008GL036784.

1. Introduction

[2] Recently continuous Global Positioning System (cGPS) observations have increased manifold in many tectonic settings. The cGPS sites provide times series of the ground motions, typically a position each day, with a horizontal accuracy of just a few millimeters. These GPS observations show clearly that the motion of the surface of the Earth is not entirely linear, that is, the steady motions are interrupted by tectonic excursions known as ‘transients’. Attempts to isolate the transients by independently removing the linear motions can be difficult when the times series are short or noisy. Here, I outline a new approach to take advantage of the strong spatial correlation in the velocities of nearby surface geodetic sites. Velocities are estimated with a block/fault model of the tectonics while simultaneously solving for parameters describing transient sources. In this way, GPS sites need neither a long history nor frequent observations in order to contribute to understanding regional kinematics and transients. The method is applied to the northern Cascadia subduction zone where the estimated locking distribution between slow slip events reveals a close relationship between the geodetic transition zone (where interseismic locking ceases at depth) and the locations of the slow-slip events (SSE). The SSEs overlap for the most part but not entirely the region that is partially locked between

the slip events. This region of the fault is likely marking the lower frictional stability transition zone.

2. Method

[3] The purpose of the method described is to invert the GPS time series to estimate simultaneously the long term linear (steady) motions of sites and short-term transients such as slow slip events, volcanic sources and earthquakes. The steady motions of the sites are described by crustal block rotations and strain rates (elastic or anelastic or both) that together predict spatially smooth variations in surface velocities, thus providing a spatial correlation among sites. An advantage over curve-fitting techniques, such as the hyperbolic method [e.g., *Szeliga et al.*, 2008], is that transient events that overlap in space and time can be distinguished. The method also provides estimates of fault locking and block rotations that have been corrected for transient motions.

[4] The inter-event (steady) geodetic surface velocities arise from a combination of crustal block rotations, elastic strain rates from locked faults and distributed permanent strain rates. Here that part of the problem is represented by a linear time series of discrete observations of position X :

$$X_{ij}(t) = X_{ij}^o + V_{ij}(t - t_o) + \varepsilon_{ij}(t) \quad (1)$$

where X_{ij}^o is the initial position of component i (east, north and up) of site j at time $t = t_o$, V_{ij} is the i^{th} component of steady velocity of site j and $\varepsilon_{ij}(t)$ represents other signals. Commonly, the velocity V is estimated by finding the best-fit slope for each time series individually. The approach used here takes advantage of the strong spatial correlation of velocities among nearby geodetic sites due to the inherent long-wavelengths of Earth deformation. The details of the model parameters related to the steady velocities are given by *McCaffrey* [1995] and *McCaffrey et al.* [2007].

[5] The type of transient addressed in this application is slow slip but the method can also be applied to earthquakes, with or without afterslip, and time-dependent volcanic sources. Slow-slip events (SSE) are thought to be due to slip on fault planes, much like earthquakes, but occur slowly enough to not radiate detectable seismic waves, except perhaps as tremor [*Dragert et al.*, 2004]. Geodetic inversions have generally solved for slip on patches of the fault and applied smoothing by specifying the covariance among nearby patches that are not independently resolved [e.g., *Segall and Matthews*, 1997; *Szeliga et al.*, 2008]. Here, instead, I use simple functions to describe the spatial and temporal distributions of slip on the

¹Department of Earth and Environmental Science, Rensselaer Polytechnic Institute, Troy, New York, USA.

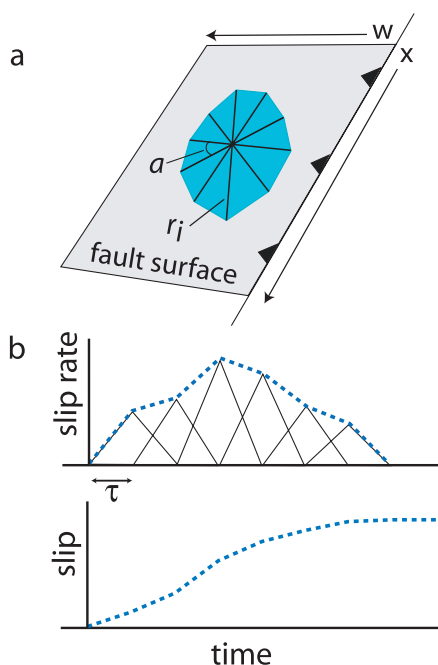


Figure 1. (a) Slip on the fault is assumed to be nominally uniform over a polygon whose vertices are formed by the distances r_i radiating from a fixed point at fixed azimuth increments a . A 10% gradient in slip rate from center to edge is introduced for numerical purposes. (b) The slip rate time history is formed by a series of overlapping triangles of fixed duration τ . Here two or three triangles with $\tau = 7$ days are used for each event.

fault surface (Figure 1) (see auxiliary material).¹ The slip rate history on the fault during an event is given by:

$$s(x, w, t) = AX(x)W(w)S(t) \quad (2)$$

where s is the slip rate on the fault at along-strike position x , down-dip position w and time t , and A is the amplitude. The spatial slip can be described by a rectangular patch, a two-dimensional Gaussian distribution or a polygon covering a portion of the fault within which slip is nominally uniform (Figure 1a), as is used here. The vertices of the polygon are parameterized by the distance of each from a central point at evenly-spaced azimuths in the $x - w$ plane (Figure 1a). For this application, the central point is fixed beneath the region of highest surface slip and the radial distances of each vertex from it form the free parameters.

[6] The time dependence $S(t)$ of the slow slip event can be set to a Gaussian function, a box-car function or a series of overlapping triangles (Figure 1). In this paper a time history comprising overlapping triangles is used, as is done for earthquake time functions [e.g., *Nabelek*, 1984]. For a slow slip event the free parameters for the time history are T_o , the origin time, and the triangle amplitudes A_i , ($i = 1, N$ where N is the number of triangles in the time function; A is given in mm/yr). The rise-time of the triangle (τ ; Figure 1b) is fixed at 7 days for all events and 2 or 3 triangles are used. The surface

displacement history is found by integrating $S(t)$ over time (Figure 1) and applying the appropriate Green's functions. Since transients in Cascadia are seen to migrate along the margin at rates of several km per day [*Szeliga et al.*, 2008], I allow the onset of slip at each site to be delayed as determined by two free parameters, a migration rate and azimuth.

3. Application to the Cascadia Subduction Zone

[7] The Juan de Fuca plate subducts eastward beneath the North American coast at ~ 40 mm/yr off Oregon and ~ 46 mm/yr off Vancouver Island (Figure 2a). Upper plate deformation at the Cascadia margin is complex, comprising several distinct crustal blocks [*Wells et al.*, 1998; *McCaffrey et al.*, 2007]. Using 13 years of survey-mode and cGPS observations, geologic fault slip rates, and earthquake slip vectors, *McCaffrey et al.* [2007] quantified the deformation through rotations of crustal blocks and along-strike variations in locking on the Cascadia plate interface. Those velocities were not corrected for slow-slip.

[8] Data used here are the daily positions of 53 cGPS sites in northernmost Oregon, Washington and Vancouver Island from years 2003.2 up to 2008.8 acquired from the Pacific Northwest Geodetic Array (www.geodesy.cwu.edu). Processing the raw data and filtering to remove instrument change offsets and seasonal signals are described by *Szeliga et al.* [2008]. Each daily position is assigned an uncertainty based on the processing (~ 2 mm for the east and north components, ~ 6 mm for the vertical). The inversions described below result in normalized rms values of 1.0, 1.2 and 1.0 for the East, North and Up components and weighted rms of 1.6, 2.0 and 5.1 mm, respectively, suggesting that the assigned uncertainties are reasonable. The best-fitting parameters are estimated using simulated annealing to minimize the sum of the reduced chi-square statistic (χ_r^2 ; sum of the squares of the weighted residuals normalized by the degrees-of-freedom) plus any penalties due to parameter constraints, such as positivity in slip, for example. Uncertainties are estimated in the end by a linear approximation to this non-linear inverse problem.

[9] The three-dimensional Cascadia slab geometry (Figure 2a) from *McCrorry et al.* [2003] is digitized at nodes approximately every 10 to 30 km in x (along strike) and about every 20 km in w (down-dip). The surface response to distributed slip on the fault is obtained first by calculating the response to unit slip at each node (Green's functions) using an elastic halfspace dislocation model [*Okada*, 1992], then convolving the Green's functions with the estimated slip at the nodes. The treatments of interseismic subduction locking and the upper plate block geometry are similar to that of *McCaffrey et al.* [2007]. The Juan de Fuca rotation pole was fixed and the estimated poles for crustal blocks are relative to North America. Because the data are consistent with the assumption that slow slip is opposite the local subduction direction, slip directions during the events are derived from the block angular velocities. Locking on crustal faults is not modeled (i.e., free slip on them is assumed).

4. Results

[10] The 3-component time series from March 2003 through September 2008 for 53 sites, comprising over 83,000 site-days of data, were used. First, an inversion

¹Auxiliary materials are available in the HTML. doi:10.1029/2008GL036784.

was run in which no transients were included – called the ‘uncorrected’ model. The 234 free parameters comprise three components of the angular velocities for 6 blocks (Figure 2a), three components of uniform horizontal strain rate tensors in 3 blocks, three parameters each for 16 locking profiles (see auxiliary material), and three time series offset parameters for each of 53 GPS sites. This inversion, that resulted in $\chi_r^2 = 1.146$, simulates what might be inferred from campaign GPS were no corrections made for slow slip events (Figure 2a).

[11] The ‘SSE-corrected’ model includes the four slow slip events of June 2004, August 2005, January 2007 and April 2008 (Figures 2b, 3, and 4). In addition to the block/locking model parameters described above, parameters for the slip

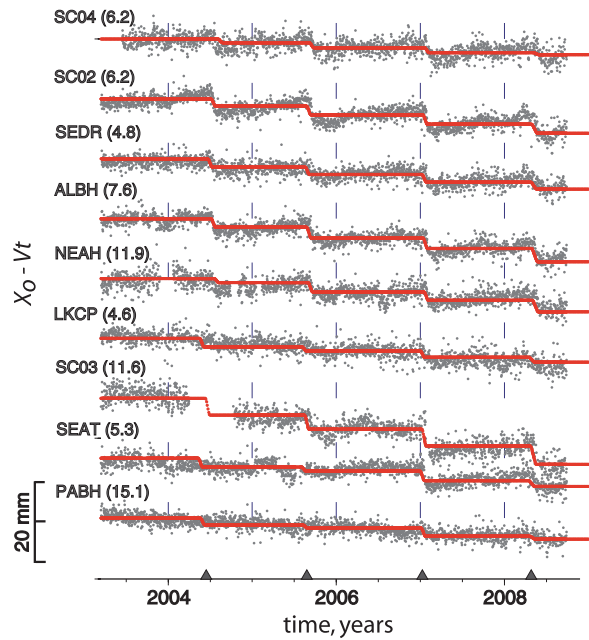
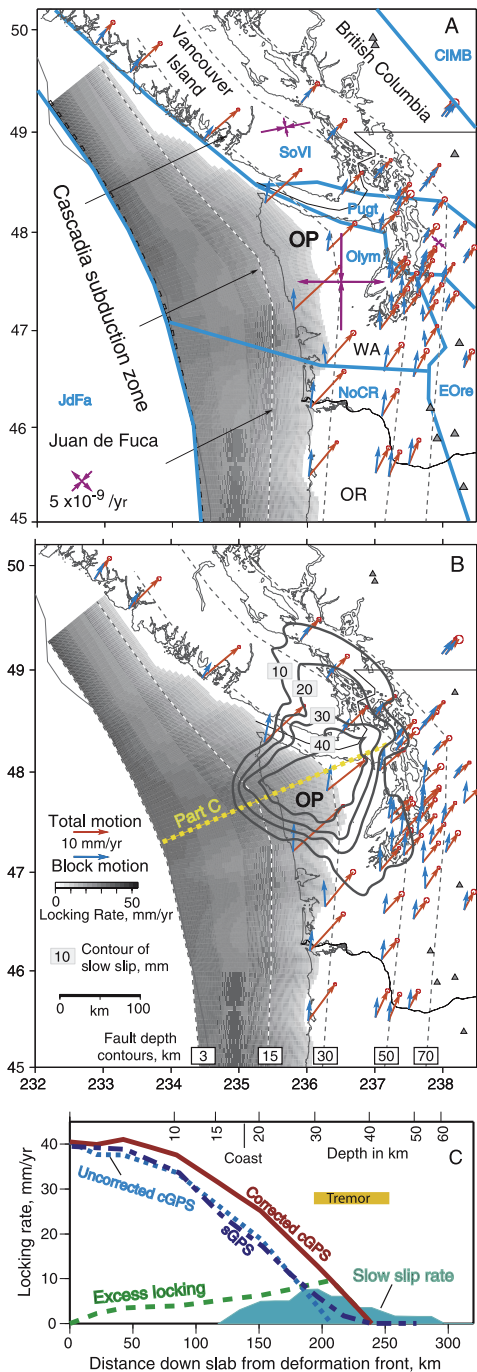


Figure 3. Examples of daily positions of east components (gray dots), labeled by site code and steady velocity (in mm/yr). Amplitude scale has linear velocity removed. Red curves show model predictions and triangles show times of slip events. Site locations shown in Figure 4a and complete set of time series are in the auxiliary material.

distribution and time history for each event included 10 radial distances, 2 triangular time function elements (3 for 2008 event), 2 migration parameters and an origin time for a total of 295 free parameters. This inversion resulted in $\chi_r^2 = 1.106$ which is 3.5% lower than the model that included no slow slip – the small variance reduction is due to the small signal-to-noise ratio of Cascadia slip events (the fits to the east components of selected sites is shown in Figure 3).

[12] The representation of the slow slip events by uniform slip over a contiguous but irregularly-shaped patch of the fault (Figure 4) results in a different appearance of slip than

Figure 2. (a) Cascadia locking distribution for case where no slow slip events are used; see legend in Figure 2b. Black arrows show velocities of Juan de Fuca plate, blue arrows show block motions, and red arrows show steady site velocities, all relative to North America. Opposing purple arrows show uniform strain rates within crustal blocks. Blocks are outlined by thick blue lines and denoted by 4-letter codes. OP, Olympic Peninsula; OR, Oregon; and WA, Washington. (b) Locking distribution for case where slow slip events have also been modeled. Dark contours labeled in mm show total slip in the four slow slip events. (c) Profile of locking and slow slip through the Olympic Peninsula (OP). Bar labeled ‘Tremor’ shows region where non-volcanic tremor is observed [Wech and Creager, 2007]. Thick curves show locking distribution when correcting cGPS for slow slip (solid) and not (dashed) and that based on uncorrected survey GPS (sGPS) [from McCaffrey et al., 2007]. ‘Excess locking’ is the difference between corrected and uncorrected locking. Filled curve is the average yearly rate of slow slip beneath this profile line over the 5.6 years studied.

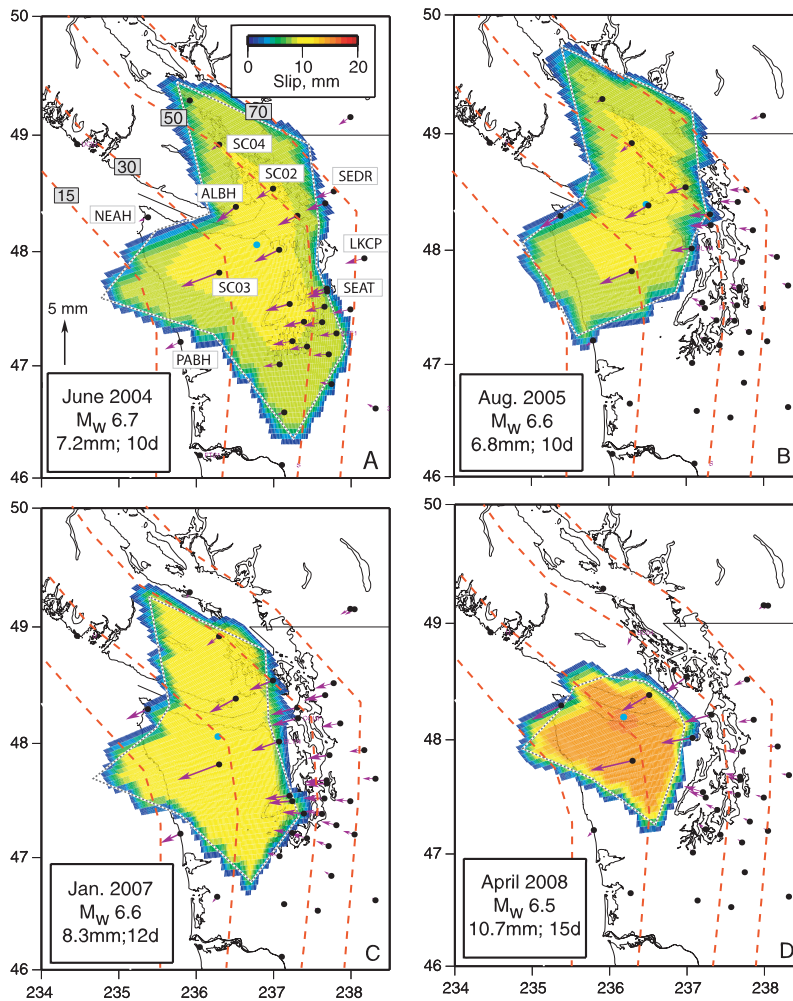


Figure 4. Slip distributions (shading) and surface displacements (purple vectors) for slow slip events. Dashed lines are subduction zone depth contours labeled in km in Figure 4a. Dots are cGPS sites operating at the time of the event. Legends give the date, equivalent moment magnitude, average slip on the fault in mm and duration of event in days. Fine dashed lines show slip polygon (fuzzy edges of slip zones are due to gridding of fault and a 10% gradient from center to edge is used).

when spatially variable slip is allowed. For the latter, damping is used to prevent patchy distributions that result when individual observation sites correlate with local slip patches (e.g., slip wavelengths can be similar to the station spacing). Compare, for example, Figures 4a and 4b to the *Szeliga et al.* [2008] solutions for the same events that have multiple, spatially disconnected slip patches (in auxiliary material). The use of a contiguous, uniform-slip patch produces fits to the time series that are satisfactory in most cases. The inter-event velocity for site SC02 (Figures 3 and 4) is underestimated by a few mm/yr which results in underestimating the offsets in the SSEs but this is level of misfit is rare. Misfits in this sense lead to lower estimates of both locking and slow slip. The remaining sites show approximate ‘stair-step’ time series when their steady velocities are removed (all time series are shown in the auxiliary material).

[13] The steady Cascadia locking distribution estimated from the uncorrected time series (Figure 2a) and that from the SSE-corrected time series (Figure 2b) are very similar except beneath the Olympic Peninsula (OP). In the time between slow slip events the plate interface beneath the OP appears to be partially locked about 10 km deeper and about 10 mm/yr

faster than average, as seen in the uncorrected cGPS or survey-mode (sGPS) result (Figure 2c; this difference is labeled as ‘Excess locking’). Velocities that are not corrected for slow slip may show locking that is too shallow. Slow slip occurs mostly in the 20 to 40 km depth range ($w \sim 150$ to 250 km; Figure 2c) which coincides with the bottom of the SSE-corrected locking (~ 40 km depth) and non-volcanic tremor (Figure 2c). The average slow slip rate (the sum of the slow slip divided by 5.6 years), at least for the area beneath land, appears to account for a large portion of the excess locking (Figure 2c). It should be noted that slow slip occurs to the northwest and south of the region examined here and some of that unmodeled slip is evident in the time series. In addition, smaller unmodeled slip events may occur within the time period examined. However, neither of these sources adds significant moment to the OP region.

[14] The steady site velocities from the SSE-corrected model are 2 to 3 mm/yr faster than average velocities above the region of slow slip. Most to all of this difference is due to the locking distribution; for example the block rotation component of site SC03, in the middle of the OP (Figure 4a), is essentially identical for the SSE-corrected and uncorrected

models while the elastic component for the SSE-corrected model is 3.3 mm/yr and 0.9 mm/yr, for east and north respectively, faster. The lack of a trade-off between block rotation and locking is probably because they are producing velocities that are nearly orthogonal throughout the southern two-thirds of the region.

5. Discussion

[15] An important feature of the Cascadia slow slip events examined is their close spatial association with the geodetic transition zone as imaged by surface geodetic data, an association that may be global [Schwartz and Rokosky, 2007]. For the SSE-corrected locking, the moment rate on the Cascadia subduction zone (for the section of the fault north of 45°N) is 9.8×10^{19} Nm/yr (using a shear modulus of 40 GPa), the average (uncorrected) rate is 9.0×10^{19} Nm/yr and the total moment released in the four slow-slip events is 4.3×10^{19} Nm. Hence the slow-slip events released over the 5.6 years is about 8% of the slip deficit accumulation (tests in the auxiliary material show a range of 7 to 10%). Locally, beneath the Olympic Peninsula, the fractional rate of moment release in slow slip is about double but it is not known why this is so. Since slow slip and tremor can be triggered by very small changes in stress on the fault [Liu and Rice, 2007], one possibility is that the topography of the OP keeps stress on the plate boundary closer to a critical value than elsewhere along the margin.

[16] Models of the mechanics of slow slip generally indicate that it may occur only within the transition where the frictional behavior of the fault goes from stick-slip (velocity weakening) at shallow depths to stable sliding (velocity strengthening) deeper along the interface [Liu and Rice, 2007]. The close association of slow slip with the geodetic transition zone observed here supports that finding if the geodetic transition is in fact also revealing the stability transition. At the Hikurangi subduction zone, New Zealand, slow slip correlates with the geodetic transition zone even through large ranges in depth from very shallow, less than 15 km, to deeper, 30 to 40 km, along strike [McCaffrey et al., 2008]. If the stability transition is also where earthquake nucleation is inhibited, then slow slip and the geodetically imaged transition zone may provide a way to find that important stability transition during the interseismic period.

6. Conclusions

[17] Recent Cascadia slow slip events can be modeled as contiguous regions of uniform slip on the fault. The four

events from 2003 through 2008 show most slip at depths where it is partially locked in the time between the events. It is thought that this region marks the transition from stick-slip behavior to stable sliding. If so, slow slip provides an observation to locate this transition zone at depth on the fault.

[18] **Acknowledgments.** The efforts of the PANGA Processing Center are essential for this work; thanks to Marcello Santillan for supplying the data. Funded by NASA and GNS Science.

References

- Dragert, H., K. Wang, and G. Rogers (2004), Geodetic and seismic signatures of episodic tremor and slip in the northern Cascadia subduction zone, *Earth Planets Space*, *56*, 1143–1150.
- Liu, Y., and J. R. Rice (2007), Spontaneous and triggered aseismic deformation transients in a subduction fault model, *J. Geophys. Res.*, *112*, B09404, doi:10.1029/2007JB004930.
- McCaffrey, R. (1995), *DEFNODE User's Guide*, Rensselaer Polytech. Inst., Troy, N. Y. (Available at <http://www.rpi.edu/~mccafr/defnode>)
- McCaffrey, R., A. I. Qamar, R. W. King, R. Wells, G. Khazaradze, C. A. Williams, C. W. Stevens, J. J. Vollick, and P. C. Zwick (2007), Fault locking, block rotation and crustal deformation in the Pacific Northwest, *Geophys. J. Int.*, *169*, 1315–1340, doi:10.1111/j.1365-246X.2007.03371.x.
- McCaffrey, R., L. M. Wallace, and J. Beavan (2008), Slow slip and frictional transition at low temperature at the Hikurangi subduction zone, *Nat. Geosci.*, *1*, 316–320.
- McCrory, P. A., J. L. Blair, D. H. Oppenheimer, and S. R. Walter (2003), Depth to the Juan de Fuca slab beneath the Cascadia subduction margin: A 3-D model for sorting earthquakes [CD-ROM], *U. S. Geol. Surv. Digital Data Ser.*, *91*.
- Nabelek, J. (1984), Determination of earthquake source parameters from inversion of body waves, Ph.D. thesis, 262 pp., Mass. Inst. of Technol., Cambridge.
- Okada, Y. (1992), Internal deformation due to shear and tensile faults in a half-space, *Bull. Seismol. Soc. Am.*, *82*, 1018–1040.
- Schwartz, S. Y., and J. M. Rokosky (2007), Slow slip events and seismic tremor at circum-Pacific subduction zones, *Rev. Geophys.*, *45*, RG3004, doi:10.1029/2006RG000208.
- Segall, P., and M. Matthews (1997), Time dependent inversion of geodetic data, *J. Geophys. Res.*, *102*, 22,391–22,410.
- Szeliga, W., T. Melbourne, M. Santillan, and M. Miller (2008), GPS constraints on 34 slow slip events within the Cascadia subduction zone, 1997–2005, *J. Geophys. Res.*, *113*, B04404, doi:10.1029/2007JB004948.
- Wech, A. G., and K. C. Creager (2007), Cascadia tremor polarization evidence for plate interface slip, *Geophys. Res. Lett.*, *34*, L22306, doi:10.1029/2007GL031167.
- Wells, R. E., C. S. Weaver, and R. J. Blakely (1998), Fore arc migration in Cascadia and its neotectonic significance, *Geology*, *26*, 759–762.

R. McCaffrey, Department of Earth and Environmental Science, Rensselaer Polytechnic Institute, Troy, NY 12180, USA. (mccafr@rpi.edu)